Airborne Analysis and Assessment of Urban Traffic Scenes from LiDAR Data – Theory and Experiments

Wei Yao[1] Stefan Hinz[2] and Uwe Stilla[1]
[1]Photogrammetry and Remote Sensing, Technische Universitaet Muenchen, Germany
[2]Computer Vision and Remote Sensing, Karlsruhe Institute of Technology, Germany
yao@tum.de stefan.hinz@kit.edu stilla@tum.de

Abstract

This paper investigates the theoretical background for LiDAR to monitor traffic from airborne platforms. An object moving with a velocity deviating from the assumptions incorporated in the scanning process will generally appear both stretched and sheared – motion artifacts. To study the impact of these deformations in airborne laser scanning (ALS) data, the analytic relations between an arbitrarily moving object and its conjugate in the ALS data have been examined and adapted to concrete airborne specifications. A complete scheme is proposed to analyze urban traffic in real-life situations. This scheme combines vehicle motion classification method successively with vehicle detection. Furthermore, the velocity of moving vehicles can be derived. The algorithmic performance was assessed with respect to reference data concurrently obtained by video camera.

1. Introduction

Transportation represents a major segment of the economic activities of modern societies which leads to adverse impact on our environment, so that the increase of transport safety and efficiency, as well as the reduction of air and noise pollution are the main task to solve in the future [1].The automatic extraction, characterization and monitoring of traffic using remote sensing platforms is an emerging field of research. Approaches rely not only on airborne video but on nearly the whole range of available sensors [2][3][4]. The principal argument for the utilization of such sensors is that they complement stationary data collectors in the sense that they deliver not only local data but also observe the traffic situation over a larger region. Finally, the measurements derived from the various sensors could be fused through the assimilation of traffic flow models.

Traffic monitoring based on optical satellite systems, however, is only possible at daytime and cloud-free conditions. Besides SAR systems [5], LiDAR can work in the night time and have certain ability to penetrate the cloud. Yet there are other difficulties inherent in the LiDAR imaging process that must be overcome to design a reasonably good approach for traffic monitoring. It is the focus of this paper to thoroughly analyze and quantify these effects and to develop an approach that is capable to detect vehicles and estimate their velocity considering the restrictions of airborne LiDAR systems. Beside the advantage mentioned above, the LiDAR system has following ones especially in view of our application:

1. The completeness of vehicle extraction using LiDAR could be increased due to the partial penetration ability of laser rays against vegetations.
2. The moving object could generate motion artifacts in the LiDAR data which are utilized to distinguish the movement and estimate the velocity.

However, there have been rare works conducted in relation to traffic analysis from ALS data so far. The research work of [6] used an airborne laser scanner coupled with digital video camera to analyze transportation corridors and acquire traffic flow information. Vehicle velocity was estimated either by analyzing motion artifacts in the laser data or by vehicle tracking in image sequences. The experiences showed that the two sensors complement each other and can provide valuable traffic flow data. The presented scheme in this paper performs a systematic research on moving vehicle indication solely relying on the point cloud acquired by airborne LiDAR. The emphasis of this paper is put on vehicle motion classification while the task of vehicle detection is assumed to be solved independently.

We summarize the theoretical background of influences caused by moving objects in airborne LiDAR data in Sect. 2. Sect.3 outlines theory of a vehicle detection and motion indication algorithm. Experiments and validations using real data are presented and discussed in Sect.4. Real data have been acquired during two flight campaigns where the sensor instrument has been parameterized such that the resulting data correspond to common tasks for city surveying.

2. Moving objects in ALS data

In an airborne LiDAR scanning process, a rotating laser pointer rapidly scans the earth's surface with continuous scan angles during its flight. While the sensor is moving it transmits laser pulses at constant intervals given by the Pulse Repetition Frequency (PRF) and receives the echoes. In Fig.1 the geometry of data acquisition is shown. The sensor is flying in a certain altitude along the dotted arrow called along-track direction. The direction which is

978-1-4244-7028-0/10/$26.00 ©2010 IEEE

oriented perpendicular to the flight path is referred to as across-track direction. The distance between sensor and target is calculated based on the stationary-world assumption, significantly moving and even accelerating objects violate this assumption and therefore the target will not be imaged "correctly". The dependencies on object velocity and acceleration components can be seen by adding the temporal component into range equation. Here it is assumed that sampling rate is consistent among all the vehicles independent of the scan angle. That is to say that all the vehicles are scanned with sufficient sampling points to represent its shape and artifact.

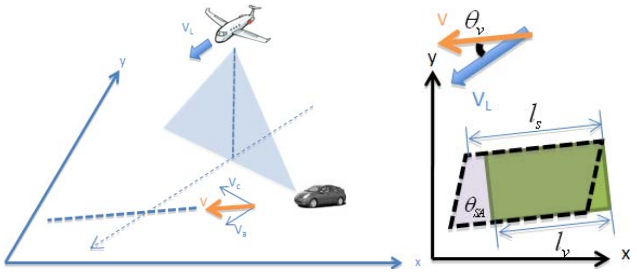

Fig.1 Moving objects undergo the scanning of airborne LiDAR

The generated shape artifacts by moving objects can be depicted in Fig.1, where the black dotted box indicates the vehicle shape obtained in the scanning process of ALS while the original vehicle is depicted as rectangle nearby. It can be perceived that the moving vehicle will be imaged as stretched parallelogram in the ALS data. θ_v is the intersection angle between the moving direction of sensor and vehicle $\in [0^\circ\ 360^\circ]$, l_s and l_v are the sensed and orignal length of vehicle, respectively; θ_{SA} is the shearing angle making vehicle be deformed as parallelogram. The analytic relations between shape artifacts and object movement parameters can be derived as

$$l_s = \frac{l_v \cdot \mathrm{v}_L}{v_L - v \cdot \cos(\theta_v)} = \frac{l_v}{1 - \frac{v}{v_L} \cdot \cos(\theta_v)} \tag{1}$$

$$\theta_{SA} = \arctan\left(\frac{v \cdot \sin(\theta_v)}{v_L - v \cdot \cos(\theta_v)}\right) + 90^\circ \tag{2}$$

where $\theta_{SA} \in (0^\circ\ 180^\circ)$ and is the left-bottom angle of observed vehicle. The imaging effects caused by the two motion components are explained in the following Sections, respectively.

2.1. Along-track motion

The target is now assumed to move with constant velocity v_a following the along-track direction. The along-track motion changes the relative velocity between sensor and object compared to the surrounding stationary world which makes the laser footprints that hit upon target displaced consistently along the target moving direction. Therefore, along-track motion leads to the stretching effect of the object shape depending on the relative velocity between target and sensor.

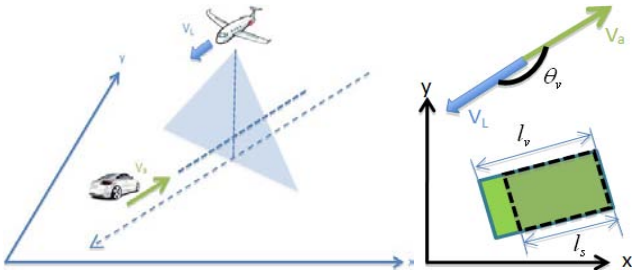

Fig.2 Along-track motion

The analytic relation between the object velocity v_a and the observed stretched length l_s can be summarized in Eq.3. Rather than the vehicle length that usually varies a lot and is not able to be exactly known in advance, the aspect ratio of vehicle is assumed to be determined easily due to its relative stability over one vehicle category. For this reason, the relation in Eq.3 is further modified to Eq.4 in order to make motion indication and velocity estimation feasible and reliable in real-life scenes.

$$l_s = \frac{l_v}{1 - \frac{v_a}{v_L}} \tag{3}$$

$$Ar_s = \frac{l_s}{w_v} = \frac{Ar}{1 - \frac{v_a}{v_L}} \tag{4}$$

where Ar_s is the sensed aspect ratio of vehicle in ALS data while Ar is the original aspect ratio of vehicle.

2.2. Across-track motion

The target is now assumed to move in across-track with a constant velocity v_c. It results in a scanline-wise linear shift of laser footprints that hit upon target towards the moving direction when sensor sweeping over, so that the observed vehicle shape in ALS data is deformed (sheared) to certain extent depending on the relative velocity between target and sensor. In Fig.3 this is shown. The analytic relation connecting the object velocity v_c with the observed shearing angle θ_{SA} through sensor velocity v_L and the intersection angle θ_v can be constructed in Eq.5.

$$\theta_{SA} = \arctan\left(\frac{1}{\frac{v_L}{v_c} - \cot(\theta_v)}\right) + 90^\circ \tag{5}$$

which is zero for stationary objects and those moving only in along-track.

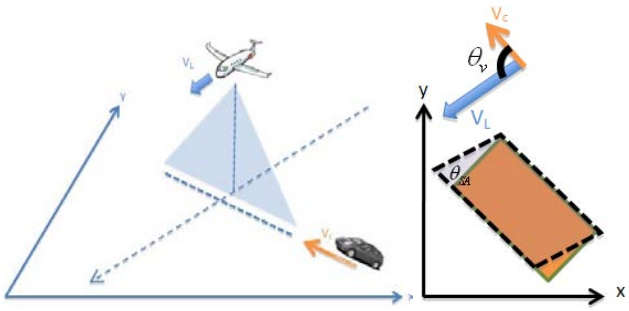

Fig.3 Across-track motion

2.3. Acceleration

In the majority of *GMTI* applications except in highways, it is assumed that vehicles travel with constant velocity and along a straight path. However, within our scope of monitoring the traffic in urban areas, the effect of acceleration is weak and can be ignored by quantitative modeling, especially for airborne LiDAR which sweeps over the vehicle itself very fast during the scanning process. The produced deformation on vehicle point distribution could not play a decisive role. It can be easily seen and verified by substituting the acceleration into the terms in Eq. 1&2. Actually, it could make the deformation too complex to be modeled in a consistent analytic form and immolate the accuracy of velocity estimation. For typical accelerations in common traffic scenarios (a_v<2m/s^2) the effect is almost zero.

2.4. Quantification of object motion Effects in airborne LiDAR data

We exemplify the above-mentioned effects for the case of a typical airborne LiDAR configuration which is applied to urban surveying task. Based on the formulae derived above, and using the system parameters as specified in first row of Tab.I, we estimate the impact of moving objects in ALS data. These investigations help to derive the boundary conditions for building up a strategy for detecting ground moving targets in airborne topographical LiDAR data.

Along-track Motion: The effect of stretching of the sampled target points due to an along-track component of the target velocity is calculated based on Eq.3. The sensed aspect ratio Ar_s of a moving object in an ALS point cloud is shown in Fig.4 as a function of intersection angle θ_v and vehicle velocity *v* where *Ar* is assumed to be 2. As can be seen, moving vehicles are stretched significantly from their real shape even for moderate along-track velocities (ca. 60% for 50 km/h). This effect dose not hamper the recognition of cars in ALS data as their stretched shape is still related to semantic information. Fig.4 also shows that the sensed aspect ratio Ar_s is becoming ambiguous when the intersection angle θ_v equals to or approaches 90° or 270° regardless of the target velocity.

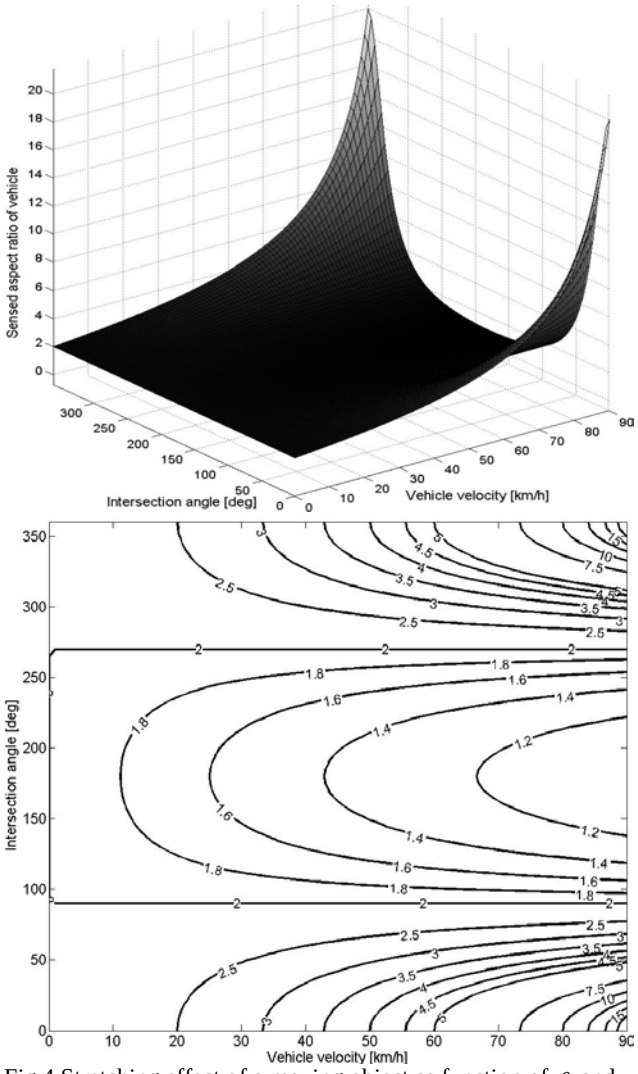

Fig.4 Stretching effect of a moving object as function of θ_v and v and its contour plot (bottom).

The Ar_s of a moving target is symmetrically distributed around the axis of $\theta_v = 180^\circ$ with moderate basin in the middle. As observed in the right corners of Fig.4, Ar_s has increased intensely as the velocity ratio of senor to target comes near to 1 which makes the velocity estimation very sensitive to noise. The along-track velocity component of object raises the ambiguity limit, since the original aspect ratio *Ar* of vehicle cannot accurately be determined for single vehicles

Across-track Motion: The effect of deformation of the shape of target points is triggered by an across-track component of the target velocity. Based on Eq.2 the shearing angle θ_{SA} of a target moving with velocity *v* is calculated. The results are presented in Fig.5 as a function of intersection angle θ_v and vehicle velocity *v*.

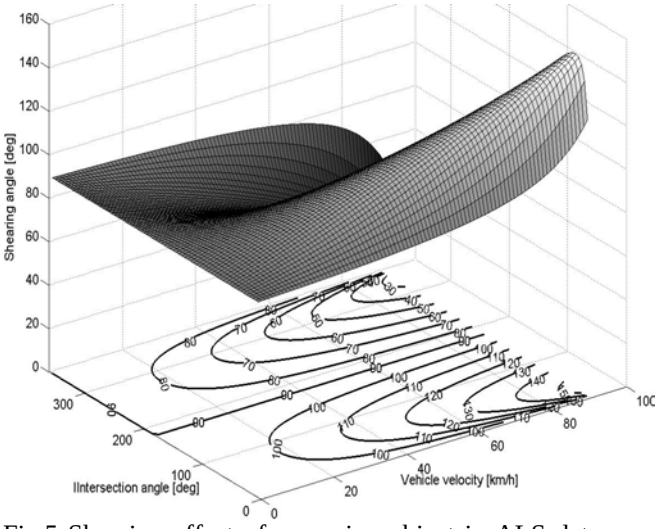

Fig.5 Shearing effect of a moving object in ALS data as function of θ_v and v.

As can be seen, the effect of across-track motion has significant influence on the geometric appearance of vehicle in ALS data. Moving vehicles are deformed (sheared) to parallelogram from their real shape even for small across-track velocities (by ca. 25° for 30 km/h). Its distribution is inversely symmetric around the axis of $\theta_v = 180^\circ$. The shearing effect on vehicle shape facilitates motion indication and allows to estimate the across-track velocity without ambiguity. It is worth to note that the occurrence of maximal shearing effect shifts from 90° to 40° for the intersection angle between the moving paths of sensor and target θ_v as the target velocity increases from zero to approach that one of sensor. Consequently, for detecting all ground moving targets which suffer from this deformation effect, the theoretic analysis on Fig.5 could provide guidance on the planning of the flight path depending on the target velocities to be estimated.

3. Vehicle detection and motion analysis

The approach proposed here to detect the moving vehicles and estimate their velocity follows the strategy of detecting all the vehicles in advance. The separation of vehicle detection from vehicle motion analysis enables us to detect not only moving vehicles but also stationary vehicles thereby giving an overview on the traffic scenario of large region scanned by airborne LiDAR. Moreover, the approach features no necessity to incorporate the prior knowledge of roads and their directions, as well as those about the appearance, location and velocity of vehicles.

Our scheme for vehicle detection and velocity estimation relies on three basic components: (1) retrieving vehicle points (Sect. 3.1); (2) modeling the vehicle shape (Sect. 3.2) and (3) an algorithm for distinguishing the vehicle motion status based on shape artifacts (Sect. 3.3).

3.1. Vehicle points retrieve

No matter whether vehicles move or not during the scanning process of the airborne LiDAR, they are modeled as bulged blob above the ground surface or elevated road. It is still not possible for us to determine the vehicle motion prior to detecting single vehicles from the scene background. Therefore, we need to firstly extract vehicle instances as complete as possible without distinguishing between dynamical statuses. It can be done by the manual inspection or automatic extraction strategy. Here we used a hybrid strategy that integrates 3-D segmentation based classification method with a context-guided approach to segment vehicle points. As easily imagined, it is generally a very difficult and demanding task, since LiDAR points are unevenly sampled upon the object surface and inherently have no topological relation at all. Experiments demonstrated that the assimilation of these two approaches can make vehicle extraction competent and robust against various clutters of urban areas.

To make sure that the extracted points for single vehicles can be further used to undergo motion analysis based on the motion artifacts described in section II, the shape preservation of extracted vehicle points is evaluated by calculating the Hausdorff distance metric between every vehicle point cluster extracted and the one in the reference. The smaller the metric is, the better the shape of extracted vehicle is preserved.

Although vehicle extraction plays a key role in view of the automatic estimation of vehicle motion, this paper will not focus on it. We refer the readers to [7],[8] for a detailed analysis of vehicle detection.

3.2. Vehicle shape parameterization

It is desirable for our task to represent original vehicle shape and motion artifacts by a unified model. The spoke model for vehicle point sets (Fig.7) is used as general framework for vehicle shape modeling due to its flexibility and efficiency. The point cloud of single vehicles is fitted with multiple connected planes used to describe the vehicle shape by two controlling parameters of each spoke - the orientation and radius. The spoke model could consistently encode geometric information for the classification of vehicle category.

However, the laser point density acquired under common conditions is not sufficient to model the vertical profile of a vehicle. The situation is even degraded by motion artifacts and the variation of scan angle. Since the motion artifacts focused on the horizontal deformation of vehicle shape, the 3D spoke model of vehicles can be projected onto horizontal plane to avoid the redundancy. Due to the limitation on the point density, we might model all vehicle categories with one spoke plane in most cases. Then, the shape parameterization is performed on the projected point sets of the vehicle spoke model by two steps:

- **Boundary tracing**: A modified convex-hull algorithm [9] is used to determine the vehicle boundary. The modification is made upon constrain the searching space of a convex hull formation to a local neighborhood. The study showed that the approach can yield satisfactory results if the point distribution is consistent throughout the dataset. Such condition could be fulfilled for the one-path ALS data which are usually considered for analyzing the object motion. The boundary tracing method for a set of vehicle points using the modified convex hull starts with the left-most point *P*. Then, we use the convex hull algorithm to find the next boundary point by only considering the points within the neighborhood of *P*, which is defined as rectangle with the dimension corresponding to the point spacing of ALS data. The approach proceeds to the newly found boundary point and repeat the step mentioned above until the point *P* is selected again, as depicted in Fig.6.
- **Boundary regularization**: Since the uneven point sampling is present in the ALS data, the traced boundary cannot be directly used to parameterize the vehicle shape. The boundary regularization is introduced to tackle the problem based on the fact that the vehicle point sets appear as parallelogram having two orientations of boundaries. The first step is to extract the points that lie on identical line segments. This is done by sequentially following the boundary points and locating positions where the slopes of two consecutive edges significantly differ. Points on these edges are grouped to one line segment. Therefore, a set of line segments $\{l_1, l_2, ..., l_n, n \geq 4\}$ from which four longest line segment $\{L_1, L_2, L_3, L_4\}$ are selected. Each of the selected line segments is fitted by the straight line. Based on the slope $M_i = -A_i/B_i$, line segments are sorted into different groups, each of which contains quasi-parallel line segments. The next step is to determine the least squares parallelogram fitting to these line segments with the constraint that the lines segments are parallel to each other within one group. The solution consists of sets of parameters required to describe four line segments, which are formed as following line equations:

$$A_i x_j + B_i y_j + 1 = 0 \qquad i = 1,2,3,4;\ j = j(i) = 1,2,3,\ldots\ n_i \tag{6}$$

with the condition: $\begin{matrix} M_1 = M_3 \\ M_2 = M_4 \end{matrix} \Leftrightarrow L_1\ (L_2)$ and $L_3\ (L_4)$ are opposite sides, where n_i is the number of points of each line segment.

Once the spoke model of a set of vehicle points is parameterized (Fig.6, right column), two parameters can be derived:

1. The angle of shear θ_{SA} of vehicle:

$$\theta_{SA} = \arctan\left(\left|\frac{M_2 - M_1}{1 + M_1 \cdot M_2}\right|\right) \tag{7}$$

2. The aspect ratio *Ar* of the parameterized vehicle points:

$$Ar = L/W \tag{8}$$

where M_1, M_2 are slopes of line segments of each group.

For certain vehicle points the parallelogram fitting could fail due to unstable sampling of LiDAR points. These vehicles emerge as e.g. trapezoid (Fig.6, third column) other than parallelogram. These vehicle points deliverer ambiguous shape features and make the motion determination troublesome, because they could e.g. belong to a stationary vehicle with missing parts. Therefore, this category of vehicle points has to be excluded and attributed to uncertain motion status prior to the motion classification step.

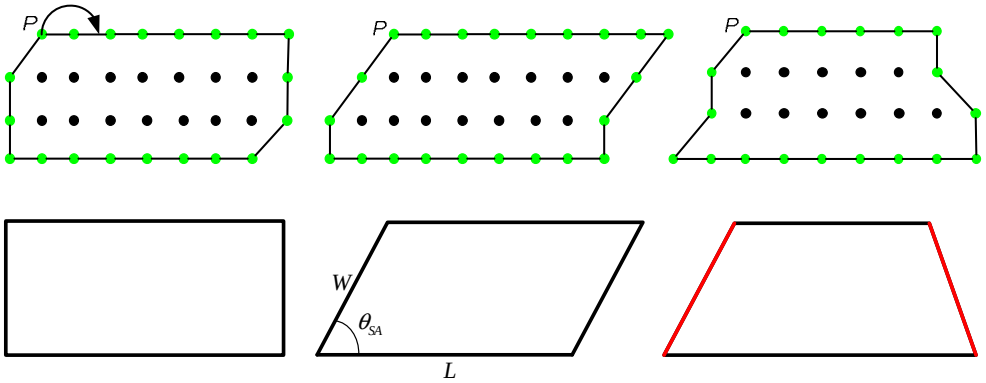

Fig .6 Vehicle shape parametrization. From left to right: stationary vehicle, moving vehicle, vehicle of ambiguous shape. Green points mark the boundary of extracted vehicle; red lines indicate the non-parallel sides of the fitted shape.

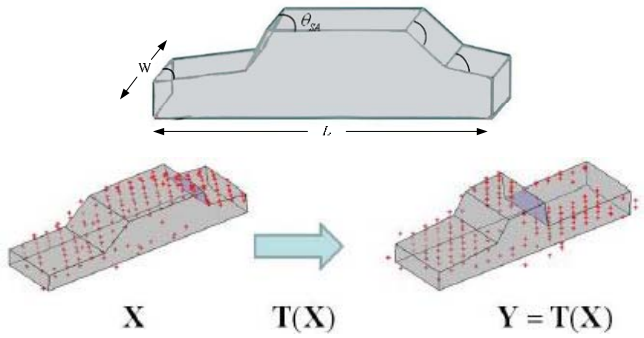

Fig.7. Vehicle spoke model and shape transformation [10]

3.3. Motion classification

A set of vehicle points can be geometrically described as spoke model with two parameters(Fig.7), whose configuration is formulated as

$$X = \begin{pmatrix} U_1 \\ . \\ . \\ U_k \end{pmatrix},\ U_i = \begin{pmatrix} \theta_{SA}^{i} \\ Ar_i \end{pmatrix} \tag{9}$$

where k denotes the number of spokes in the model. The vehicle shape variability is nonlinear and can be represented as a transformation space. Thus, the similarity between vehicle instances can be measured by group distance metric. The classification framework for distinguishing vehicle categories can be adapted to motion classification schema based on shape features of vehicle points.

Consequently, a new vehicle configuration Y can be obtained by a transformation of X written in matrix form: $Y=T(X)$

where $T = \begin{pmatrix} M_1 & . & 0 \\ . & . & . \\ 0 & . & M_k \end{pmatrix}$, $M_i = \begin{pmatrix} R_i & 0 \\ 0 & e^{ai} \end{pmatrix}$, R_i denotes the 2-D rotation acting on the angle of shear θ_{SA}, e^{ai} denotes the scale acting on Ar. By varying T, any vehicle shape X (motion status) may be represented in T as the transformation of an identity atom(Fig.7). Since the Cartesian product of Lie group elements is a Lie group and T is the Cartesian product of transformation matrices M_i acting on the individual spokes, T forms a Lie group G[11]. The intrinsic mean μ of a set of transformation matrices $T_1, T_2, \ldots, T_n$ of vehicle shapes is defined as

$$\mu = \arg\min \sum_{k=1}^{n} d(T, T_k)^2 \tag{10}$$

where $d(\cdot,\cdot)$ denotes Riemannian distance and $d(T_1,T_2) = \left\|\log(T_1^{-1}T_2)\right\|$ where $\|\cdot\|$ is the Frobenius norm of the algebra elements. Analogous to the principle components of a vector space, there exists 1-parameter sub-group $H_v(t)$ called the principle geodesic curve [12] which describes the essential variability of the data points lying on the manifold. The parameter t sweeps out a 1-parameter sub-group $H_v(t)$ of the Lie group G. For any $g \in G$, the distance between g and $H_v(t)$ is defined as

$$d(g, H_v) = \min d(g, \exp[A_v(t)]),\quad t \in \Re \tag{11}$$

The first principle geodesic curve for elements of a Lie group G is defined as the 1-parameter subgroup $H_{v^{(1)}}(t)$, where $v^{(1)} = \arg\min \sum_{i=1}^{n} d^2(\mu^{-1}g_i, H_v)$

(12)

Let $p_{i,1}$ be the projection of $\mu^{-1}g_i$ on $H_{v^{(1)}}$, and define $g_i^{(1)} = p_{i,1}^{-1}\mu^{-1}g_i$. The higher k-th principle geodesic curve can be determined recursively based on Eq.12. It has been confirmed that Lie group PCA can better describe the variability of data that is inherently nonlinear[12].

The motion analysis can be formulated as a binary classification problem. The input to the Lie distance classifier comprises a set of labeled samples from two vehicle categories $C_j\,(j=1,2)$ - moving and stationary. The intrinsic mean μ_j and the principal geodesics $H_{v^{(n)}}$ are computed for each C_j using the samples. Once the principal geodesics are available, the classification of an unlabeled vehicle sample x can be performed by finding the category with the closest distance on the first principal geodesics to x. The corresponding motion status of a vehicle j is found by

$$j^* = \arg\min \left\|\log(H_{j,v^{(1)}}^{-1}\mu^{-1}x)\right\|,\quad j \in \{1,2\} \tag{13}$$

The classification of vehicle status can successfully run based solely on the first principal geodesics. Although there are significant variations in shape over one category, the first principal geodesics $H_{v^{(1)}}$ is assumed to summarize the essential shape features of vehicle points in view of distinguishing the motion statuses.

4. Experiment and validation

In order to verify the validity of the theory and the detection scheme, two flight campaigns (Fig.8a&b) with airborne LiDAR systems have been conducted over city areas in Europe to compare the theoretical derivations with real data (Tab.I). Please note that the following experiments are intended to yield a performance characterization of our approach when applied to real-life traffic scenarios acquired by LiDAR under common conditions (not optimized for the detection of moving objects). The campaigns were conducted to validate and possibly improve the theory with help of real conditions. During the data acquisition the reference data were also made. For the both flights, an optical video camera mounted on the same

plane was used to provide concurrent observations. They exhibited the traffic situation at the time of acquisition. The velocities of moving vehicles can be accurately estimated by vehicle tracking.

	Flight velocity	Point density	Flight height	Swath	View mode	Time
Data I	100km/h	8 pts/ m^2	275m	320m	nadir	11:05
Data II	145km/h	5 pts/ m^2	420m	480m	forward	10:26

Table I Configuration parameters for two experimental campaigns

The flights investigated realistic scenarios with significant along- and across-track motion components. Fig.8 shows the output of applying the detection scheme. Detected stationary vehicles are plotted as green while detected moving ones are plotted as blue at their position with moving directions. Vehicles of the uncertain category excluded from the classification scheme are plotted as red.

To get quantitative estimates of the quality of velocity determination from airborne LiDAR data, the velocity corresponding to the along-track elongation in LiDAR data v_e^a has been derived based on the original aspect ratio *Ar* of the vehicle. Similar experiments have been carried out for determining across-track velocity based on the shape distortion. Tab.II summarized the validation results of the experiments. The velocity of detected moving vehicles v_e is finally estimated by $v_e = \sqrt{\left(v_e^a\right)^2 + \left(v_e^c\right)^2}$ and compared to the velocity reference v_r.

As can be seen in Fig.8, there is a good agreement between the detection results and the reference measurements for most of vehicles in the two datasets (approx. 60-70% detection rate), so that the theoretical background of detection and velocity estimation seems justified. The velocities derived from the motion artifacts are representative for all the cars travelling on that road. The values for the 2nd test site (Fig.8b) are reasonable for this section of the urban road and correspond very well to the speed value of vehicles moving towards the traffic light. Although there might be some inaccuracies included in the measurements the results show a good match of theory and real measurements. However, the tests tent to further show that the detection rate and the accuracy for velocity estimation drop down for smaller cars or those ones moving slowly. This can mainly be explained by the limited spatial resolution and the higher sensitivity of shape parametrization to noise. Current airborne LiDAR data have resolutions ranging from 0.5m to 2m, so that, in certain situations, the target's point is mixed with the background. Hence, the point sampling rate as well as the backscatter is biased towards smaller values, which makes detection and estimation less robust. Furthermore, vehicles moving with a low velocity would be more likely to have an inaccurate parameterized shape. Fortunately, the problem is to some extent alleviated, since vehicles with unambiguous shape have already been removed prior to the motion classification step and labeled as uncertain class.

Buses and smaller transport vehicles dominated the test site. Although the accuracy of motion status and velocities derived this way is limited, it provides a good representation of the whole traffic situation and the velocity distribution in urban areas.

Target #	v_r km/h	v_e km/h	Δv km/h
1	42.3	39.8	2.5
2	48.6	45.4	3.2
3	65.5	63.8	1.7
4	20.5	17.1	3.4
5	28.6	24.3	4.3
6	15.7	21.3	5.6

Tabel II Comparison of estimated velocities with reference data

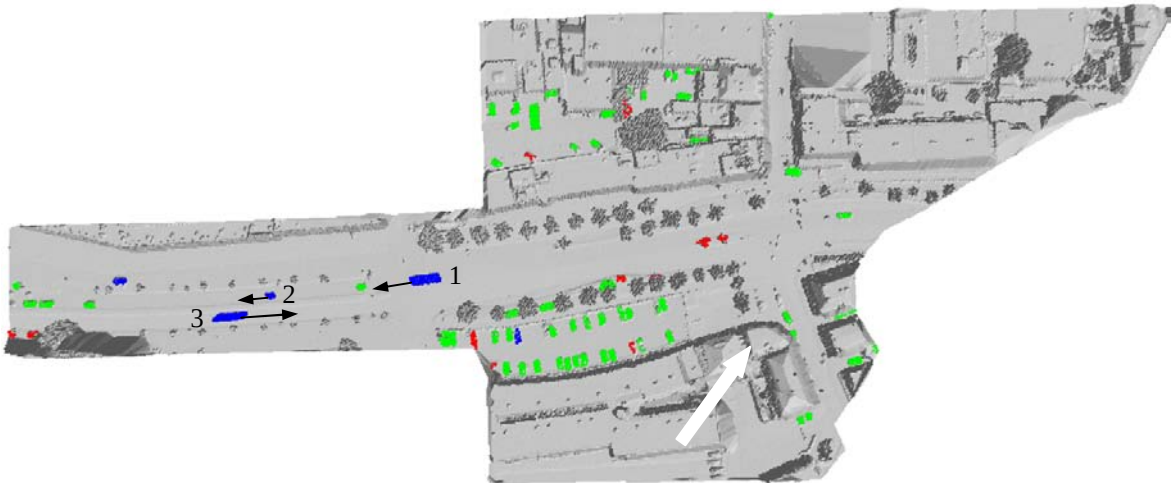

(a)

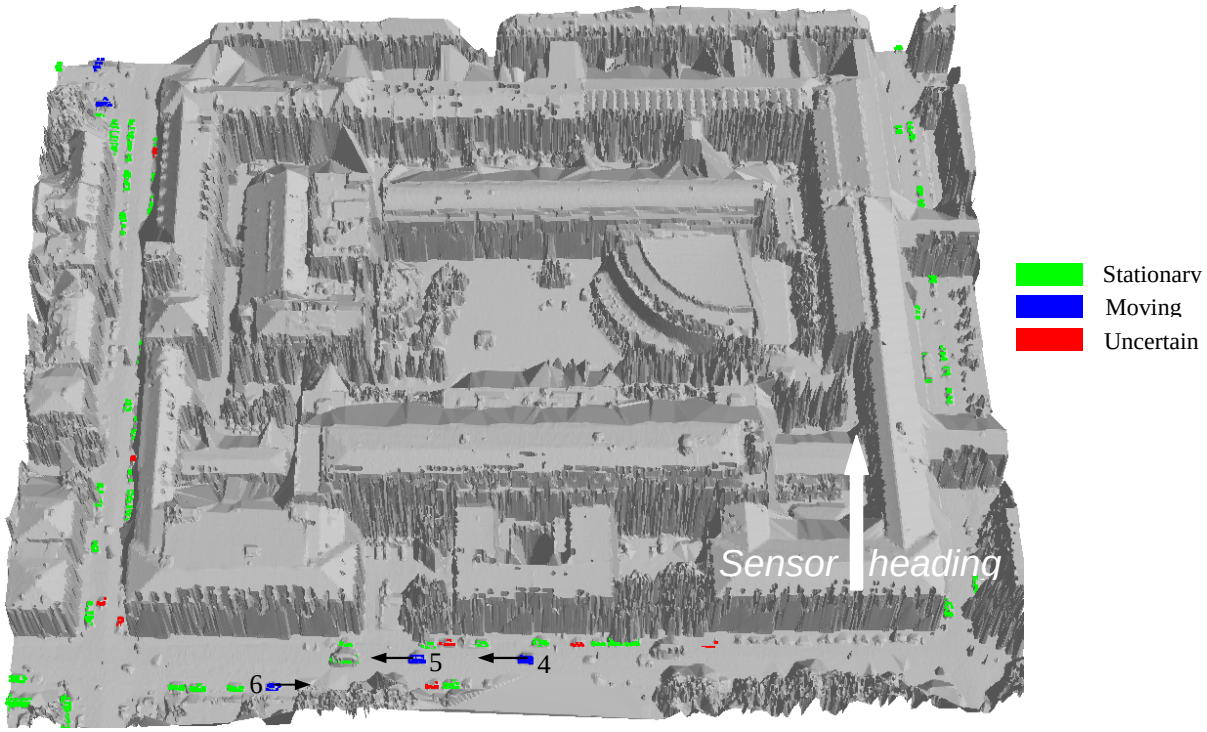

(b)

Fig.8 Results for vehicle motion classification and velocity estimation using real ALS datasets of two urban areas, a) Enschede, the Netherlands; b) Munich, Germany (displayed as overlaid with DSM)

5. Acknowledgement

The authors would like to thank Prof. Vosselman from International Institute for Geo-Information Science and Earth Observation-ITC for providing the experimental dataset of Enschede, the Netherlands.

6. References

[1] D. Rosenbaum, F. Kurz, U. Thomas, S. Suri. and P. Reinartz, Towards automatic near real-time traffic monitoring with an airborne wide angle camera system. European Transport Research Review, 2008.

[2] S. Hinz, D. Lenhart, and J. Leitloff, Traffic extraction and characterisation from optical remote sensing data. The Photogrammetric Record, 23(124): 424-440, 2008.

[3] X. Jin, and C.H. Davis, Vehicle detection from high-resolution satellite imagery using morphological shared-weight neural networks. Image and Vision Computing, 25(9): 1422-1431, 2007.

[4] M. Kirchhof, U. Stilla, Detection of moving objects in airborne thermal videos. ISPRS Journal of Photogrammetry and Remote Sensing, 61(3-4):187-196,2006.

[5] F. Meyer, S. Hinz, A. Laika, D. Weihing, and R. Bamler, Performance analysis of the TerraSAR-X Traffic monitoring concept. ISPRS Journal of Photogrammetry and Remote Sensing, 61(3-4): 225-242, 2006.

[6] C.K. Toth, and D. Grejner-Brzezinska, Extracting dynamic spatial data from airborne imaging sensors to support traffic flow estimation. ISPRS Journal of Photogrammetry and Remote Sensing, 61(3-4): 137-148, 2006.

[7] W.Yao, S. Hinz, and U. Stilla, Automatic Vehicle Extraction from Airborne LiDAR Data of Urban Areas aided by Geodesic Morphology, Pattern Recognition Letters, in press, 2010.

[8] W.Yao, S. Hinz, and U. Stilla, 2009. Object extraction based on 3D-segmentation of LiDAR data by combining mean shift and normalized cuts: two examples from urban areas, 2009 IEEE/ISPRS Urban Remote Sensing Joint event: URBAN 2009-URS 2009.

[9] R.A. Jarvis, Computing the shape hull of points in the plane, IEEE Computing Society Conference on Pattern Recognition and Image Processing, New York, pp. 231–241, 1977.

[10] P. Yarlagadda, O. Ozcanli. and J. Mundy, Lie group distance based generic 3-d vehicle classification,. ICPR 2008. 19th International Conference on Pattern Recognition, pp. 1-4, 2008.

[11] W. Rossman, 'Lie Groups: An introduction through linear groups. Oxford University Press, 2002.

[12] P.T Fletcher, L. Conglin, and S. Joshi, Statistics of shape via principal geodesic analysis on Lie groups, IEEE Computer Society Conference on Computer Vision and Pattern Recognition. Proceedings, vol.1, pp. 95-101 2003.